Published August 17, 2009

Myosin-driven peroxisome partitioning in *S. cerevisiae*

Andrei Fagarasanu,[1] Fred D. Mast,[1] Barbara Knoblach,[1] Yui Jin,[3] Matthew J. Brunner,[3] Michael R. Logan,[1] J.N. Mark Glover,[2] Gary A. Eitzen,[1] John D. Aitchison,[4] Lois S. Weisman,[3] and Richard A. Rachubinski[1]

[1]Department of Cell Biology and [2]Department of Biochemistry, University of Alberta, Edmonton, Alberta T6G 2H7, Canada
[3]Life Sciences Institute, Department of Cell and Developmental Biology, University of Michigan, Ann Arbor, MI 48109
[4]Institute for Systems Biology, Seattle, WA 98103

In *Saccharomyces cerevisiae*, the class V myosin motor Myo2p propels the movement of most organelles. We recently identified Inp2p as the peroxisome-specific receptor for Myo2p. In this study, we delineate the region of Myo2p devoted to binding peroxisomes. Using mutants of Myo2p specifically impaired in peroxisome binding, we dissect cell cycle–dependent and peroxisome partitioning–dependent mechanisms of Inp2p regulation. We find that although total Inp2p levels oscillate with the cell cycle, Inp2p levels on individual peroxisomes are controlled by peroxisome inheritance, as Inp2p aberrantly accumulates and decorates all peroxisomes in mother cells when peroxisome partitioning is abolished. We also find that Inp2p is a phosphoprotein whose level of phosphorylation is coupled to the cell cycle irrespective of peroxisome positioning in the cell. Our findings demonstrate that both organelle positioning and cell cycle progression control the levels of organelle-specific receptors for molecular motors to ultimately achieve an equidistribution of compartments between mother and daughter cells.

Introduction

Membrane-bound organelles organize the eukaryotic cell into distinct compartments that are each specialized for specific cellular functions. Compartmentalization allows a range of different processes to occur simultaneously within optimal microenvironments to increase the overall metabolic efficiency of cells. To maintain the advantages of compartmentalization, eukaryotic cells have evolved molecular mechanisms to ensure the faithful inheritance of their organelles during cell division.

The yeast *Saccharomyces cerevisiae* divides asymmetrically by budding. The accurate inheritance of its organelles is achieved by delivery of a portion of its organelles to the bud concomitant with retention of the remaining organelles in the mother cell (Fagarasanu and Rachubinski, 2007). This feature makes detection and isolation of mutants defective in organelle partitioning easier in budding yeast than in cells that divide by median fission, thus facilitating investigation of the spatial and temporal control of organelle motility.

The bud-directed movement of organelles is mediated by class V myosins, which are motors specialized in carrying cargo along actin filaments. The amino termini of all class V myosins contain a conserved motor domain that generates actin-based movements, whereas their divergent carboxyl termini form a globular domain called the tail that is specialized in capturing various organelles. Myo2p and Myo4p are the *S. cerevisiae* class V myosins (for reviews see Reck-Peterson et al., 2000; Bretscher, 2003; Pruyne et al., 2004). Myo4p is involved in the movement of cortical ER (Estrada et al., 2003), whereas Myo2p powers the bud-directed movement of most other membrane-bound organelles, including Golgi elements (Rossanese et al., 2001), the vacuole (Ishikawa et al., 2003; Tang et al., 2003), peroxisomes (Hoepfner et al., 2001; Fagarasanu et al., 2006a), and mitochondria (Itoh et al., 2002, 2004; Boldogh et al., 2004; Altmann et al., 2008). Myo2p also drives the polarized transport of secretory vesicles, which is essential for cell growth (Govindan et al., 1995; Schott et al., 1999), and carries the plus ends of cytoplasmic microtubules into the bud for orientation of the nucleus before mitosis (Yin et al., 2000).

Ensuring the efficient transport of the different types of organelles carried by Myo2p requires tight control and coordination of Myo2p's attachment to and detachment from different

Correspondence to Richard A. Rachubinski: rick.rachubinski@ualberta.ca

Abbreviations used in this paper: CSM, complete supplement mixture; G6PDH, glucose-6-phosphate dehydrogenase; MBP, maltose-binding protein; mRFP, monomeric RFP; pA, protein A.

The Rockefeller University Press $30.00
J. Cell Biol. Vol. 186 No. 4 541–554
www.jcb.org/cgi/doi/10.1083/jcb.200904050

Published August 17, 2009

organelles. Importantly, distinct Myo2p functions are genetically dissectible within the Myo2p tail. For example, mutations in the Myo2p cargo-binding domain were found that specifically disrupt either vacuole inheritance or polarized secretion (Schott et al., 1999; Catlett et al., 2000). Therefore, it was proposed that each organelle has its own Myo2p-specific receptor/adaptor that binds to a specific region in the Myo2p tail. Receptor proteins that physically connect Myo2p to its organelle cargoes have been shown to be indeed different and specific for each type of organelle (Beach et al., 2000; Ishikawa et al., 2003; Itoh et al., 2004; Fagarasanu et al., 2006a; Arai et al., 2008; Lipatova et al., 2008). Interestingly, although most yeast organelles are carried by the same motor, Myo2p, they move to distinct locations at different times in the cell cycle (Fagarasanu et al., 2006b; Pashkova et al., 2006). For example, at cytokinesis, both late Golgi elements and peroxisomes relocate to the mother–bud neck where Myo2p accumulates. In contrast, vacuoles do not display Myo2p-dependent movements at this stage of the cell cycle, and no vacuolar structures are found at the mother–bud neck. Also, late compartments of the Golgi follow Myo2p to the shmoo tips in G1-arrested cells, which is in contrast to peroxisomes and vacuoles (Rossanese et al., 2001; Tang et al., 2003; Fagarasanu et al., 2006a). Thus, Myo2p associates with each type of organelle at a different and specific time in the cell cycle. The position of Myo2p receptors as mediators between the various organelles and the molecular engine driving their movement makes them ideally suited as regulatory targets for the organelle-specific patterns of movement occurring during the cell cycle.

We previously identified Inp2p as the peroxisome-specific receptor for Myo2p (Fagarasanu et al., 2006a). The levels of Inp2p fluctuate during the cell cycle in a pattern that correlates with the dynamics of peroxisome inheritance observed in wild-type cells (Fagarasanu et al., 2006a, 2007). Inp2p levels are low during early budding when peroxisomes are first observed to perform vectorial movements toward the bud and peak in medium-sized budded cells when most peroxisomes are inserted into daughter cells. Later in the cell cycle, when about half of the peroxisomes have been delivered to the bud, Inp2p levels start to decrease and return to basal values before cytokinesis (Fagarasanu et al., 2006a,b). Inp2p does not associate uniformly with all peroxisomes but accumulates preferentially on a subset of peroxisomes (Fagarasanu and Rachubinski, 2007). A correlation exists between the levels of Inp2p on different peroxisomes and their segregation fates, as only peroxisomes containing detectable amounts of Inp2p are selectively carried to the daughter cell (Fagarasanu et al., 2006a). These findings show that the availability of Inp2p on the peroxisomal membrane is an important determinant for the timing of Myo2p's attachment to peroxisomes. How Inp2p–Myo2p interactions are regulated is currently unknown.

In this study, we identify the surface region of the Myo2p tail devoted to binding Inp2p and show that this region partially overlaps the region that binds secretory vesicles. By introducing point mutations in the peroxisome-binding region of Myo2p, we artificially uncoupled peroxisome inheritance from cell cycle progression to study the regulation of Inp2p by cell cycle–dependent and organelle positioning–dependent cues. Inp2p accumulates aberrantly on most peroxisomes in the mother cell if peroxisome inheritance is abolished. Our findings suggest that the inheritance of peroxisomes involves feedback mechanisms that regulate the levels of Inp2p relative to the positioning of peroxisomes in the dividing cell. We also show that Inp2p is a phosphoprotein whose level of phosphorylation is coupled to the cell cycle. Given that common principles govern the partitioning of all organelles (Weisman 2003, 2006; Fagarasanu and Rachubinski, 2007; Li and Nebenführ, 2008; Peng and Weisman, 2008; for review see Pruyne et al., 2004), our findings point to the existence of regulatory events affecting the activity of organelle-specific receptors for molecular motors in response to organelle positioning and cell cycle progression that help to achieve an equidistribution of each organelle type between mother cell and daughter upon cell division.

Results

Isolation of mutants of the Myo2p globular tail defective in peroxisome inheritance

The globular tail of Myo2p is composed of subdomains I (residues 1,131–1,309 and 1,528–1,574) and II (residues 1,310–1,527; Fig. 1; Pashkova et al., 2005, 2006). Analysis of the surface residues of the Myo2p tail to identify regions of high sequence conservation among the class V myosins from phylogenetically distant organisms led to the discovery of several patches of conserved residues in both subdomains I and II (Pashkova et al., 2006). Conserved surface residues generally indicate sites of protein–protein interaction. Therefore, the conserved patches on the surface of the Myo2p cargo-binding domain are likely to be regions that attach to specific cargoes. Indeed, the vacuole-binding site on Myo2p occupies a small region in subdomain I, whereas the residues required for Myo2p attachment to secretory vesicles reside within subdomain II (Fig. 1; Catlett and Weisman, 1998; Schott et al., 1999; Catlett et al., 2000; Pashkova et al., 2005, 2006).

Following this reasoning, we set out to identify the peroxisome-binding domain on the surface of Myo2p by first screening cells harboring single point mutations in the conserved exposed regions of the Myo2p tail for defects in peroxisome inheritance (Fig. 1). To do this, we systematically introduced the various *myo2* alleles previously constructed by Pashkova et al. (2006; Table S2) as sole copies of the *MYO2* gene in cells expressing Pot1p-GFP to label peroxisomes (see Materials and methods). Cells were scored using a stringent all or none criterion for the presence of peroxisomes within buds using 3D confocal microscopy (see Materials and methods). Two point mutations, Y1415E and W1407F, in subdomain II of the globular tail were observed to induce severe defects in peroxisome distribution (Figs. 1 and 2). Interestingly, Y1415 resides in the region of the Myo2p tail specialized in binding secretory vesicles (Fig. 1; Pashkova et al., 2006). Quantification showed that when the bud volume reached 0–24% of the mother cell volume (small-budded cells), only 21% and 39% of the buds of the *myo2-Y1415E* and *myo2-W1407F* mutants, respectively, contained at least one peroxisome. In contrast, 84% of

Published August 17, 2009

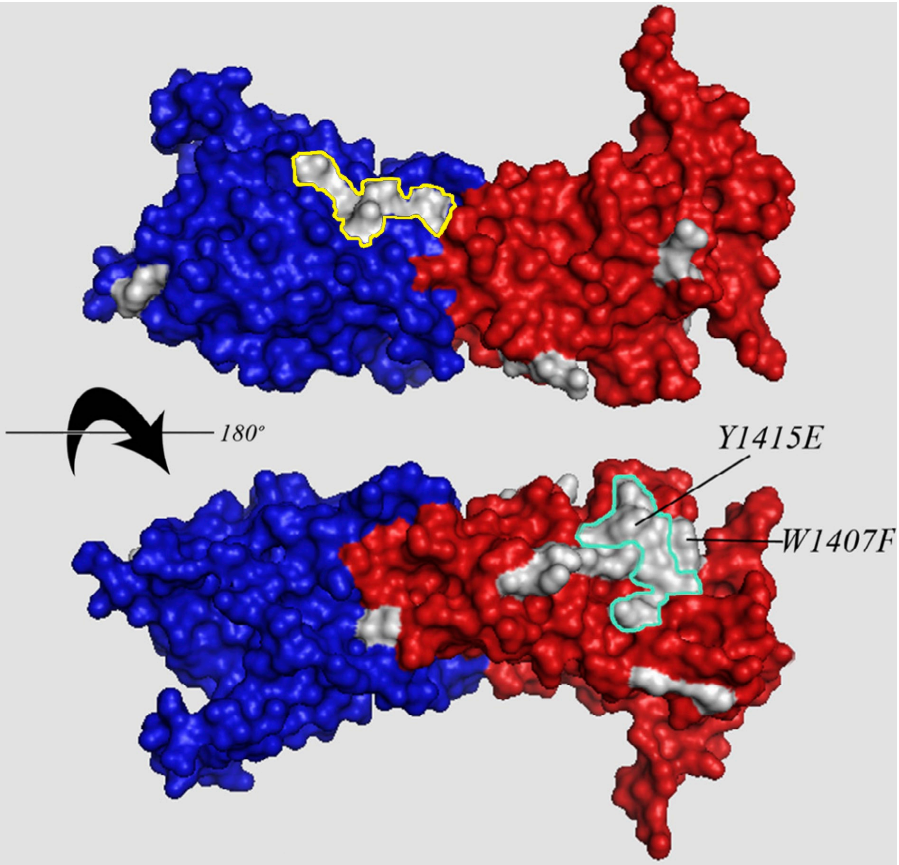

Figure 1. **Surface representation of the Myo2p globular tail.** Subdomains I and II are shown in blue and red, respectively. The mutated, conserved surface residues initially screened for defects in peroxisome inheritance are shown in white. The yellow outline demarcates the vacuole-binding site, and the teal outline demarcates the secretory vesicle–binding site.

small buds of cells with the wild-type *MYO2* gene had peroxisomes (Fig. 2 B). When the bud volume reached 24–48% of the mother cell volume (large-budded cells), only 28% and 62% of the buds of the *myo2-Y1415E* and *myo2-W1407F* mutants, respectively, displayed peroxisomal fluorescence, as compared with 98% for cells with the wild-type *MYO2* allele at the same bud sizes (Fig. 2 B).

To delineate the peroxisome-binding domain on Myo2p, we systematically replaced surface residues in the region neighboring Y1415 and W1407 with alanine (see Materials and methods) and assessed the ability of the resultant mutants to sustain peroxisome transport to buds (Fig. 2 and Table S2). Two additional substitutions, Y1483A and E1484A, were observed to disrupt the transport of peroxisomes to daughter cells (Fig. 2 B). Quantification of rates of peroxisome inheritance showed that only 33% and 47% of small-budded cells and 61% and 70% of large-budded cells of the *myo2-Y1483A* and *myo2-E1484A* strains, respectively, displayed peroxisomal fluorescence within buds. Another mutation, *myo2-K1408A*, displayed a slight defect in peroxisome distribution, with 64% of small buds and 88% of large buds containing peroxisomes. This result may suggest that K1408 is part of the peroxisome-binding region of Myo2p; however, care should be taken in making such a conclusion because the ε-ammonium of the K1408 side chain is predicted to form a hydrogen bond with the backbone carbonyl oxygen of F1334 (Fig. 2 A). Therefore, the effect of the K1408A substitution on peroxisome partitioning could be caused by a destabilization of the local architecture in subdomain II of the Myo2p tail.

Mutants of Myo2p defective in peroxisome inheritance display decreased affinity for Inp2p

If Y1415, W1407, Y1483, and E1484, whose mutation affects peroxisome transport to the bud, form a region on the surface of Myo2p specialized in binding peroxisomes, we expect mutations in these amino acids to decrease the affinity of Myo2p for its peroxisome-specific receptor, Inp2p. We have previously shown direct interaction between GST–Myo2p and maltose-binding protein (MBP)–Inp2p fusion proteins made in *Escherichia coli* (Fagarasanu et al., 2006a). We used a similar approach to quantify the interaction between Inp2p and the various Myo2p point mutants initially tested by microscopy for defects in peroxisome inheritance (Fig. 3 A). To improve the solubility of the MBP–Inp2p fusion protein, only amino acids 241–705 of Inp2p were used so as to exclude its predicted membrane-spanning region (amino acids 211–239) while retaining the region between amino acids 241 and 705 capable of interacting with Myo2p (Fagarasanu et al., 2006a). Myo2p-Y1415E, Myo2p-W1407F, Myo2p-Y1483A, and Myo2p-E1484A displayed decreased affinity for Inp2p as compared with the wild-type Myo2p tail (Fig. 3 A). Also, Myo2p-K1408A was slightly impaired in its ability to interact with Inp2p. Interestingly, some Myo2p point mutants had an increased affinity for Inp2p when compared with the wild-type Myo2p tail, indicating that regions outside the Inp2p-binding domain of Myo2p may negatively regulate the Inp2p–Myo2p interaction.

We also performed yeast two-hybrid analysis to test the ability of the various Myo2p mutants to interact with Inp2p

Published August 17, 2009

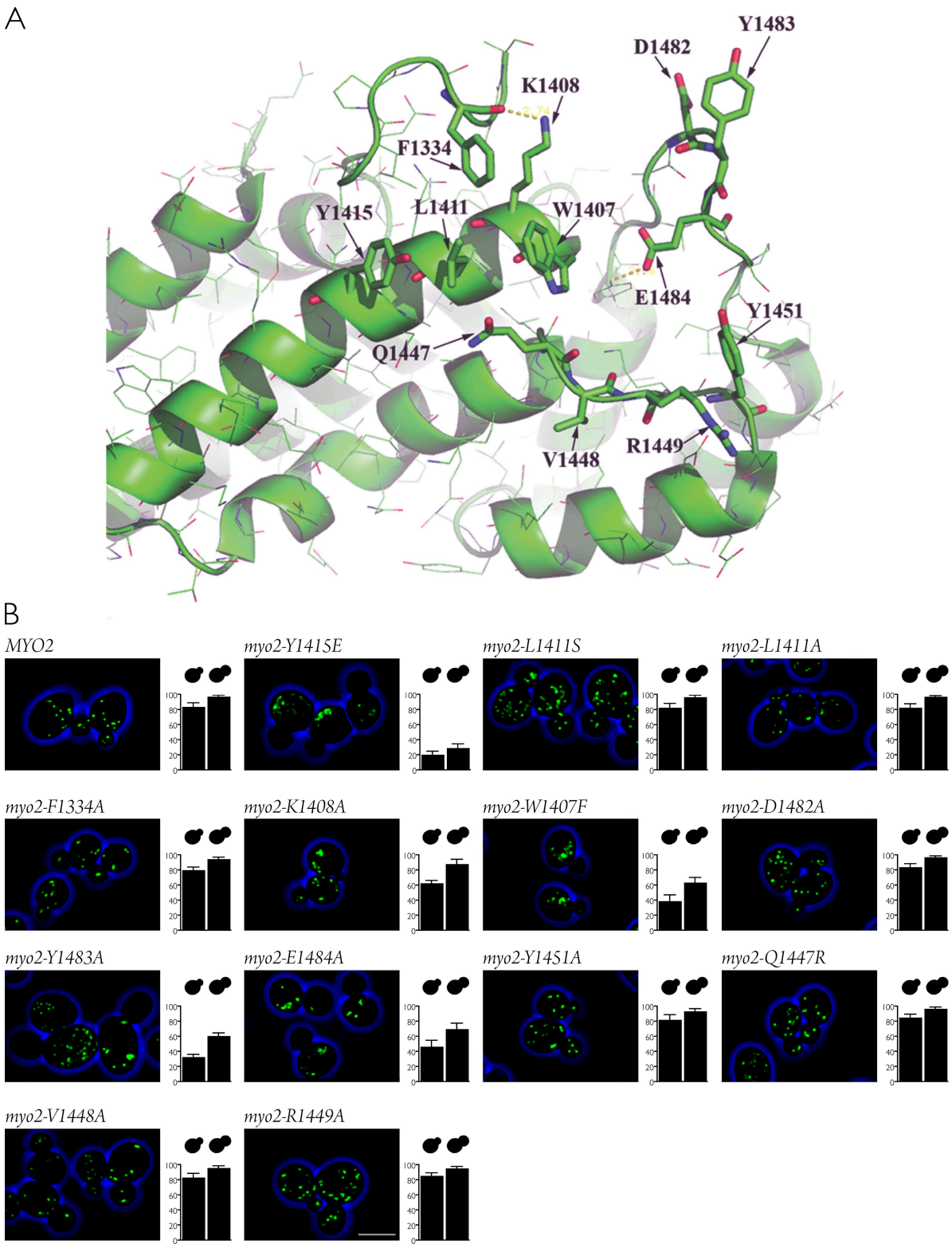

Figure 2. **Screening mutations in Myo2p for defects in peroxisome inheritance.** (A) Ribbon diagram of a portion of subdomain II of Myo2p highlighting the amino acids that were mutated. (B) Quantification of peroxisome inheritance. The percentages of buds containing peroxisomes at each size category were plotted. Quantification was performed on at least 50 budded cells from each category. Graphic results show the means ± SEM of three independent experiments. Bar, 5 µm.

in vivo. Consistent with both microscopy-based quantification of peroxisome inheritance (Fig. 2 B) and in vitro binding (Fig. 3 A), Myo2p-Y1415E, Myo2p-W1407F, Myo2p-Y1483A, and Myo2p-E1484A displayed less affinity for Inp2p than did wild-type Myo2p (Fig. 3 B). Interestingly, the L1411R mutation in the secretory vesicle–binding region of Myo2p also disrupted

Published August 17, 2009

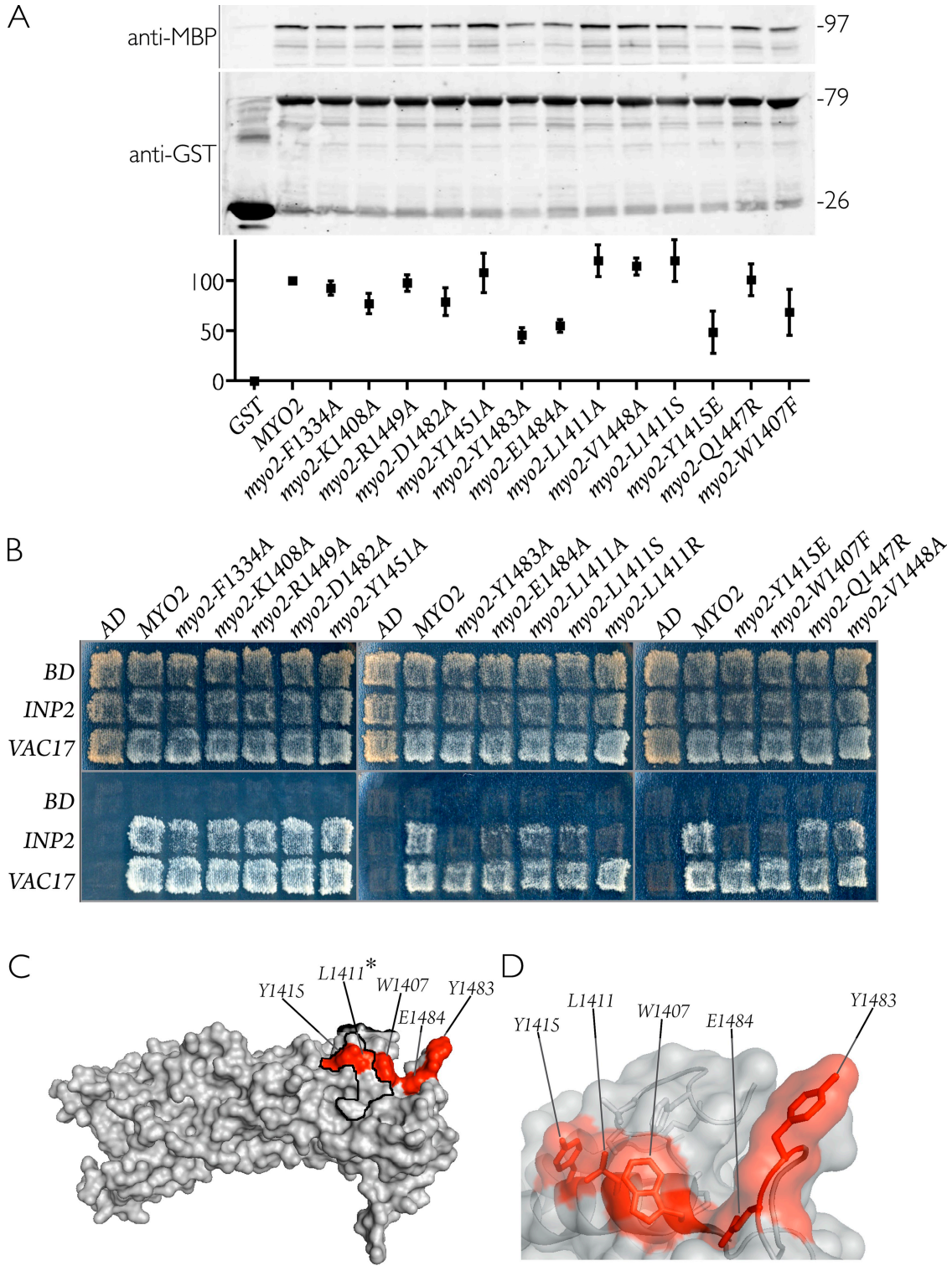

Figure 3. **Mutants of Myo2p defective in peroxisome inheritance display decreased affinity for Inp2p.** (A) Glutathione Sepharose beads containing either GST fused to the cargo-binding tail of wild-type or mutant Myo2 proteins or GST alone were incubated with extracts of *E. coli*–synthesized MBP–Inp2p. (top) Bound MBP–Inp2p was analyzed by immunoblotting with anti-MBP antibodies. (middle) Total GST–Myo2p or GST protein levels were visualized by immunoblotting with anti-GST antibodies. Numbers at right denote the approximate sizes of proteins in kilodaltons. (bottom) Quantification of bound MBP–Inp2p, normalized to wild type and expressed as percent bound, was performed by densitometry. Graphic results show the means ± SEM of three independent experiments. (B) Myo2p point mutations specifically disrupt the ability of Myo2p to interact with Inp2p (peroxisomes) but not with Vac17p (vacuoles) in a yeast two-hybrid assay. Total growth of strains (top) and growth arising specifically from protein interaction (bottom) are shown. The pattern presented is representative of seven independent experiments. AD, activation domain; BD, binding domain. (C) Crystal structure of the Myo2p globular tail with the positions of point mutations that showed either weak or no interaction with Inp2p highlighted in red. The asterisk at L1411 indicates that the L1411R mutation was able to disrupt the Myo2p–Inp2p interaction in the yeast two-hybrid assay. The secretory vesicle–binding region is outlined in black. (D) Semitransparent surface view of the Myo2p structure overlaid on a ribbon diagram displaying the side chains of residues (red) implicated in binding Inp2p.

Published August 17, 2009

interaction between Myo2p and Inp2p (Fig. 3 B); however, this mutation was not tested for defects in peroxisome inheritance because it does not support yeast viability (Pashkova et al., 2006). The inability of L1411R to bind Myo2p in the yeast two-hybrid assay could potentially extend the peroxisome-binding region of the Myo2p tail to the L1411 residue (Fig. 3, C and D). However, the other two mutations at L1411 that were tested, i.e., Myo2p-L1411A and Myo2p-L1411S (Fig. 2 B), preserved their ability to interact with Inp2p in yeast two-hybrid analysis (Fig. 3 B). Moreover, both the L1411S and L1411R mutations have been shown to severely affect yeast cell growth (Pashkova et al., 2006), indicating that the L1411S substitution is sufficient to disrupt the attachment of Myo2p to secretory vesicles. The effect of the leucine to arginine mutation at L1411 in disturbing the Myo2p–Inp2p interaction may therefore reflect a steric occlusion of the Inp2p-binding site in the Myo2p tail resulting from the long arginine side chain's hindrance of the ability of Inp2p to gain access to the neighboring amino acids, i.e., Y1415 and W1407, rather than a direct involvement of L1411 in attachment to Inp2p. The results of both in vitro binding and in vivo yeast two-hybrid analysis agree well with the findings of our microscopy analysis, wherein *myo2-Y1415E*, *myo2-W1407F*, *myo2-Y1483A*, *myo2-E1484A*, and, only partially, *myo2-K1408A* exhibited defects in peroxisome localization to the bud. This strong correlation demonstrates a clear relationship between the strength of interaction between Myo2p and Inp2p and the efficiency of peroxisome inheritance.

Myo2p point mutants defective in peroxisome inheritance are not impaired in vacuolar or mitochondrial inheritance

There is a valid concern that the identified Myo2p point mutants defective in peroxisome distribution not only impair the process of peroxisome inheritance but in fact alter the overall structure of the Myo2p tail. To test the specificity of these Myo2p mutants for peroxisome inheritance, we examined whether they retained the ability to segregate other organelles.

The distribution of mitochondria was followed with the mitochondrion-specific fluorescent label MitoTracker red. The distribution of mitochondria in cells harboring one of the four *myo2* alleles, *myo2-Y1415E*, *myo2-W1407F*, *myo2-Y1483A*, and *myo2-E1484A*, identified as being compromised in peroxisome inheritance, was essentially the same as that observed for cells expressing wild-type *MYO2* (Fig. 4 A). The segregation of vacuoles, labeled by the vacuole-specific fluorophore FM4-64, was also unchanged in these point mutants (Fig. 4 B). The observation that the *myo2-Y1415E*, *myo2-W1407F*, *myo2-Y1483A*, and *myo2-E1484A* alleles support both vacuole and mitochondria distribution clearly shows that these mutations do not affect the overall structure of Myo2p. Moreover, the specificity of these mutants in altering peroxisome distribution strongly suggests that the steady-state levels of the Myo2p mutant proteins are likely to be normal.

Interestingly, the *myo2-Y1415E* mutation confers temperature sensitivity in that it supported growth at 23°C but caused severe growth defects at 30°C (Fig. 4 C). This is consistent with the previously determined requirement of Y1415 for the polarized distribution of secretory vesicles, the only known essential cargo of Myo2p (Pashkova et al., 2006). However, other *MYO2* mutations, i.e., *myo2-W1407F*, *myo2-Y1483A*, and *myo2-E1484A*, supported growth at both 23°C and 30°C with the same efficiency as the wild-type *MYO2* allele (Fig. 4 C), indicating that these amino acyl residues are outside the secretory vesicle–binding region of Myo2p (Fig. 4 D).

Collectively, our findings demonstrate that residues Y1415, W1407, Y1483, and E1484 define the surface region of the Myo2p tail devoted to binding peroxisomes. This region resides in subdomain II of the Myo2p globular tail and partially overlaps the region that binds secretory vesicles (Fig. 4 D; Pashkova et al., 2006; Lipatova et al., 2008). Because single point mutations in the peroxisome-binding region are sufficient to cause a significant defect in peroxisome inheritance, all four residues must cooperate to anchor Myo2p securely to the peroxisomal membrane during bud-directed movement.

Inp2p aberrantly decorates peroxisomes in mother cells of a *myo2* strain mutant for peroxisome inheritance

The newly identified *myo2* mutants are the only strains reported so far in which peroxisome delivery to the bud is impaired despite the presence of an intact *INP2* gene. Cells harboring such a mutant *myo2* allele as the sole copy of the *MYO2* gene produce buds that lack peroxisomes but have a normal cell cycle, thus artificially dissociating peroxisome partitioning from cell cycle progression. An analysis of the dynamics of Inp2p in these cells would therefore permit an evaluation of the relative contributions made by cell cycle progression and peroxisome partitioning to the regulation of Inp2p. We used confocal microscopy to analyze the localization of a genomically encoded fluorescent chimera of Inp2p and GFP (Inp2p-GFP) relative to the distribution of a fluorescent peroxisomal marker, monomeric RFP (mRFP) tagged with a peroxisome-targeting signal 1 (mRFP-SKL). We restricted this analysis to strains containing either the wild-type *MYO2* allele or the mutant allele *myo2-Y1483A*, which exhibits the greatest impairment in peroxisome distribution without a concomitant defect in the targeting of secretory vesicles.

Consistent with our previous study (Fagarasanu et al., 2006a), the Inp2p-GFP signal in cells containing the wild-type *MYO2* gene was observed to be polarized and its intensity to be cell cycle dependent (Fig. 5 A). The Inp2p-GFP signal in unbudded cells was below the threshold of detection, and only cytoplasmic autofluorescence was seen. Upon bud formation, Inp2p-GFP fluorescence was detected and colocalized with mRFP-SKL. The amounts of Inp2p on individual peroxisomes varied dramatically, with only a subset of peroxisomes displaying detectable Inp2p-GFP fluorescence. Inp2p-labeled peroxisomes were delivered to the bud and congregated at the bud tip. Inp2p was detected on peroxisomes in mother cells only when buds were small. This resulted in a highly polarized Inp2p-GFP fluorescent signal along the mother–bud axis. The Inp2p-GFP signal was weak at cytokinesis and concentrated in those peroxisomes that relocated to the mother–bud neck region.

In contrast, in cells harboring the *myo2-Y1483A* mutation in which peroxisome partitioning is disrupted (Fig. 5 B), most peroxisomes in mother cells were decorated by detectable amounts

Published August 17, 2009

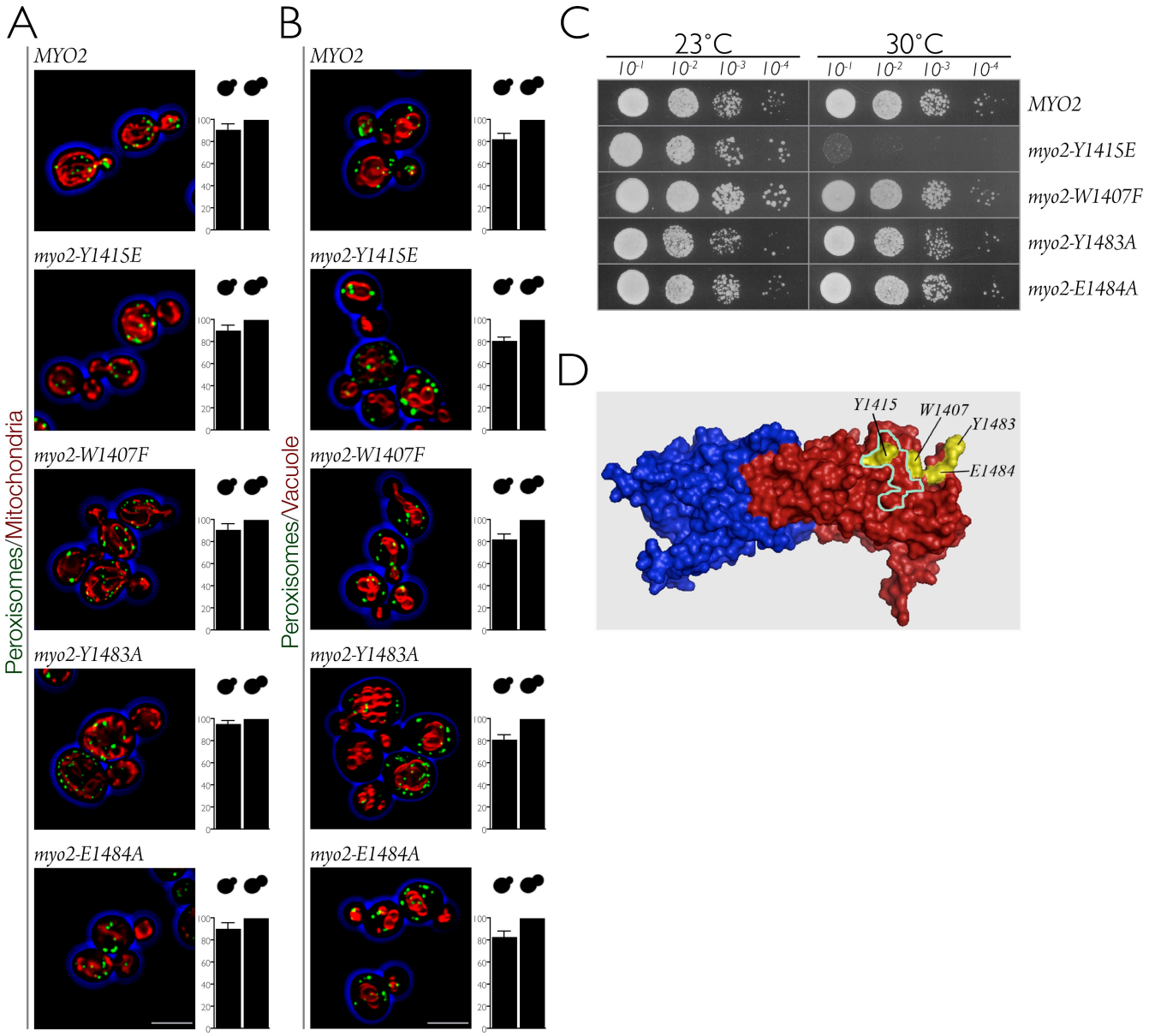

Figure 4. **Myo2p point mutants defective in peroxisome inheritance are not impaired in vacuolar or mitochondrial inheritance.** Cells expressing wild-type *MYO2* or mutant *myo2* were grown in SCIM to induce peroxisome formation, and confocal images were captured. (A and B) Peroxisomes were labeled with Pot1p-GFP, mitochondria were labeled with MitoTracker red (A), and vacuoles were labeled with FM4-64 (B). Quantification of mitochondria and vacuole inheritance was performed as in Fig. 2 B. Graphic results show the means ± SEM of three independent experiments. Bars, 5 µm. (C) Growth of cells expressing wild-type *MYO2* or mutant *myo2* on glucose-containing YPD medium. Cells were grown to mid-log phase in liquid YPD, and equal amounts of cells were serially diluted 10-fold onto YPD agar and incubated at 23 or 30°C. (D) Surface representation of the Myo2p globular tail, indicating the regions that bind peroxisomes (yellow) and secretory vesicles (teal). Subdomains I and II are shown in blue and red, respectively.

of Inp2p-GFP. Importantly, the presence of Inp2p-GFP on most peroxisomes was not the result of accumulating Inp2p-GFP during preceding cell cycles, as no Inp2p-GFP fluorescence was observed in unbudded cells of the *myo2-Y1483A* strain. Heterogeneity in the number of peroxisomes per cell was also observed in the *myo2-Y1483A* mutant, which may be the result of partitioning defects. Irrespective of the number of peroxisomes in a *myo2-Y1483A* mutant cell, Inp2p was detectable on essentially all peroxisomes of mother cells, resulting in an aberrantly depolarized distribution of Inp2p-GFP. Interestingly, the number of Inp2p-GFP–labeled peroxisomes and the signal intensity for Inp2p-GFP were decreased in those mother cells of the *myo2-Y1483A* strain in which the transfer of some peroxisomes to the bud had occurred. However, irrespective of the outcome of peroxisome inheritance, Inp2p levels decreased significantly at the end of the cell cycle.

Regulation of Inp2p levels and posttranslational modification by peroxisome positioning–dependent and cell cycle–dependent cues

The presence of Inp2p-GFP on most peroxisomes in the *myo2-Y1483A* mutant is suggestive of an overall increase in Inp2p levels during the cell cycle when peroxisome inheritance is impaired. We have previously reported that Inp2p levels vary with

Published August 17, 2009

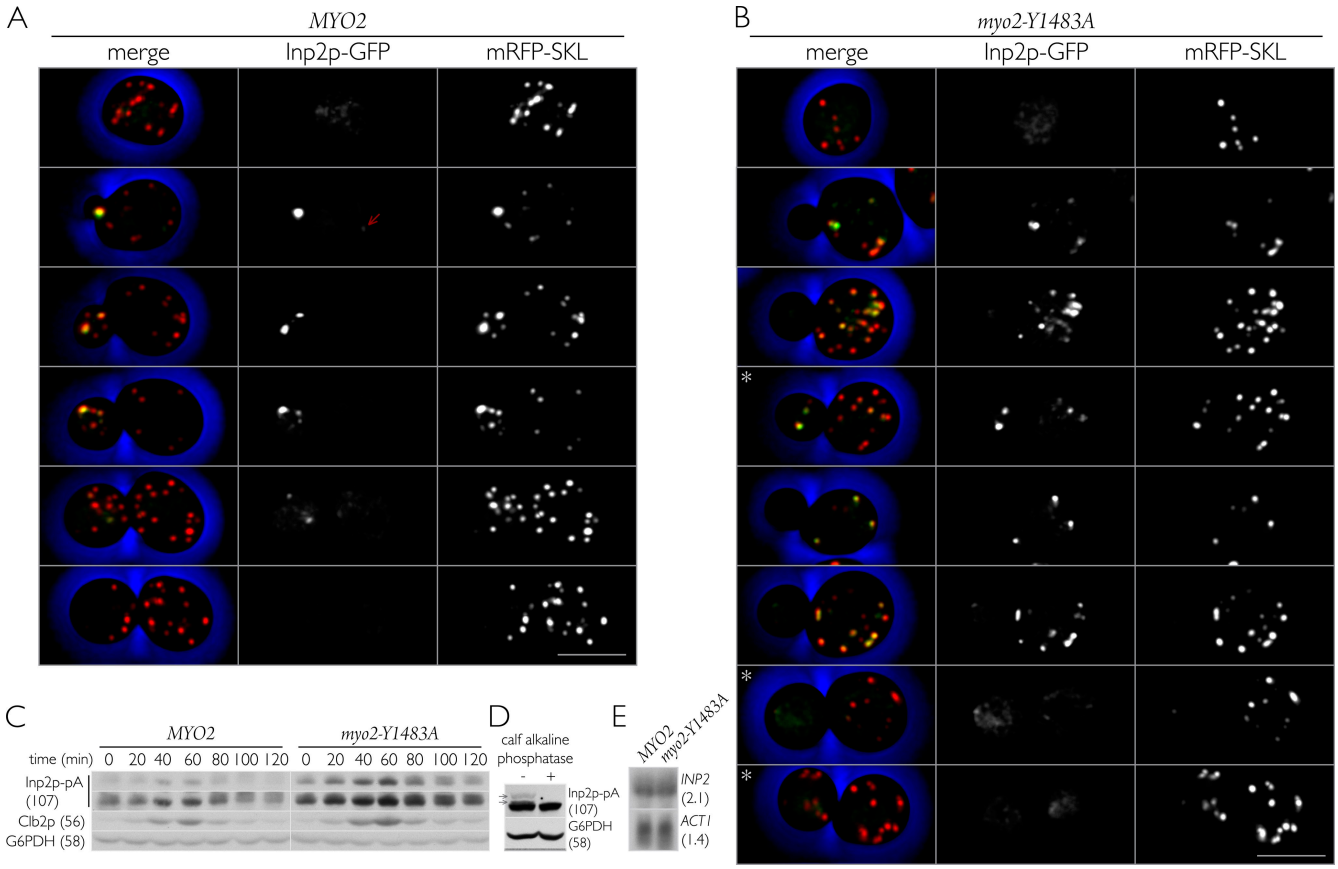

Figure 5. **Dynamics of Inp2p in cells defective in peroxisome transfer to buds.** (A and B) Inp2p accumulates on most peroxisomes in mother cells of *myo2* mutants defective in peroxisome inheritance. Cells harboring the *MYO2* gene (A) or *myo2-Y1483A* mutation (B) and expressing Inp2p-GFP and peroxisomal mRFP-SKL were grown in YPD to mid-log phase, and confocal images were captured. Left panels show the merged image of the middle and right panels. The red arrow indicates a peroxisome in a mother cell of the *MYO2* strain that contains a detectable amount of Inp2p-GFP. Asterisks indicate *myo2-Y1483A* mutant cells that have delivered peroxisomes to their buds. Bars, 5 µm. (C) Inp2p levels are increased in cells defective in peroxisome inheritance. Cells harboring either *MYO2* or the *myo2-Y1483A* mutant allele and expressing Inp2p-pA were grown in YPD and synchronized in G1 by addition of α factor (0 min). After removal of α factor, cells were incubated at 23°C in YPD. Samples were collected at the times indicated, and total cell lysates were prepared and analyzed by immunoblotting with rabbit IgG to detect Inp2p-pA and antibodies recognizing the cyclin Clb2p or G6PDH. Clb2p monitors progression through the cell cycle. G6PDH serves as a protein loading control. Detection of Inp2p-pA was for short (top) and long (bottom) exposures. The short exposure facilitates the observation of more slowly migrating phosphorylated forms of Inp2p. (D) Inp2p is phosphorylated. Total cell extracts of wild-type cells expressing Inp2p-pA were treated with water (−) or calf intestine alkaline phosphatase (+). Immunoblot analysis was performed using rabbit IgG to detect Inp2p-pA (arrows indicate the more slowly migrating species of Inp2p-pA) and anti-G6PDH antibodies. (C and D) Numbers in parentheses denote the approximate sizes of proteins in kilodaltons. (E) Northern blot analysis of total RNA from *MYO2* and *myo2-Y1483A* strains grown in YPD to exponential phase. Blots were hybridized to probes from the coding regions of the *INP2* and *ACT1* genes. *ACT1* RNA serves as a loading control for total RNA. Numbers in parentheses denote the approximate sizes of transcripts in kilobases.

the cell cycle, peaking ∼60 min after release from α factor–induced G1 arrest (Fagarasanu et al., 2006a). We assessed the levels of a genomically encoded Inp2p–protein A (pA) chimera (Inp2p-pA) in immunoblots of whole cell lysates from cell cycle–synchronized cells harboring either wild-type *MYO2* or the mutant *myo2-Y1483A* allele (Fig. 5 C). Notably, cells expressing the *myo2-Y1483A* mutation exhibited elevated levels of Inp2p-pA at all stages of the cell cycle compared with cells containing the wild-type *MYO2* allele. Because Inp2p levels are increased in cells with compromised peroxisome inheritance, we conclude that the cellular concentration of Inp2p is regulated by peroxisome positioning–dependent cues, i.e., where peroxisomes are in the cell.

Our experiments also showed that Inp2p-pA from both the wild-type *MYO2* and the mutant *myo2-Y1483A* strains migrated as multiple species on SDS-PAGE (Fig. 5, C and D). To determine whether this migration pattern was caused by post-translational modification of Inp2p-pA by phosphorylation, we treated cell lysates with alkaline phosphatase. This resulted in a collapse of the multiple Inp2p-pA species into a single, faster migrating species, demonstrating that Inp2p is indeed phosphorylated (Fig. 5 D). Phosphorylation of Inp2p-pA was coupled to the cell cycle and more pronounced at its beginning and end, whereas Inp2p at the peak of its expression 60 min after release from α factor arrest migrated as a single, fast migrating species in both *MYO2* wild-type cells and *myo2-Y1483A* mutant cells (Fig. 5 C). The observation that the timing of Inp2p phosphorylation was indistinguishable for both the wild-type *MYO2* strain and the *myo2-Y1483A* mutant strain (Fig. 5 C) suggests that there are temporally distinct phosphorylation events of Inp2p that are coordinated by cell cycle–dependent cues.

Published August 17, 2009

The increased levels of Inp2p in the *myo2-Y1483A* mutant strain could be the result of increased Inp2p synthesis, decreased Inp2p degradation, or a combination of the two. Therefore, we assessed the steady-state levels of *INP2* transcript in both wild-type cells and *myo2-Y1483A* mutant cells to test whether Inp2p synthesis is regulated by peroxisome positioning–dependent cues. Northern blot analysis revealed equal levels of *INP2* transcript in cells expressing either wild-type *MYO2* or the mutant *myo2-Y1483A* allele (Fig. 5 E). Therefore, the increased levels of Inp2p in the *myo2-Y1483A* mutant are not the result of increased transcription of the *INP2* gene but rather reflect a posttranscriptional change at either the translational or posttranslational level.

The polarized distribution of Inp2p-GFP observed in wild-type cells could suggest that only a select subset of peroxisomes can accumulate Inp2p, which results in their transfer to the daughter cell. However, the observation that Inp2p is distributed over most, if not all, peroxisomes in *myo2-Y1483A* mutant cells is consistent with a model in which all peroxisomes can accumulate Inp2p, and Inp2p levels in the mother cell are reduced upon delivery of peroxisomes to the daughter cell. To test this model, we followed the dynamics of Inp2p-GFP in cells lacking the dynamin-like protein Vps1p. Cells lacking Vps1p typically contain only one enlarged peroxisome, probably because of inefficient peroxisome fission (Hoepfner et al., 2001). During cell division, the large peroxisome present in *vps1Δ* cells emits a tubular projection that passes through the mother–bud neck into the daughter cell. This peroxisomal tubule eventually undergoes fission, resulting in two peroxisomes: one located in the mother cell and the other in the bud (Hoepfner et al., 2001). Inp2p-GFP in small-budded cells was present over the entire peroxisomal tubule, but its distribution was asymmetrical, with Inp2p being concentrated on that part of the peroxisomal tubule present in the bud (Fig. 6 A). However, in cells where the elongated peroxisome divided, the Inp2p-GFP signal was not detectable in the mother cell, and Inp2p-GFP decorated only the peroxisome in the bud (Fig. 6 A). In contrast, in the *myo2-Y1483A* mutant lacking Vps1p, the one or two peroxisomes that were present remained in the mother cell and were decorated by Inp2p-GFP (Fig. 6 A). Interestingly, we never observed elongated peroxisomes in this Myo2p mutant, suggesting that elongation of the enlarged peroxisome observed in *vps1Δ* cells carrying wild-type Myo2p is the result of pulling forces exerted by Myo2p–Inp2p transport complexes on the peroxisomal membrane (Fagarasanu et al., 2006b).

We have previously shown that overproduction of Inp1p, a protein involved in the attachment of peroxisomes to the cell cortex, retains peroxisomes at fixed cortical positions in the mother cell, thereby preventing their transfer to the daughter cell (Fagarasanu et al., 2005). We analyzed the distribution of Inp2p-GFP in cells overexpressing *INP1*. Similarly to what was observed in *myo2-Y1483A* cells, overproduction of Inp1p led to an aberrantly depolarized Inp2p-GFP signal, with Inp2p decorating most peroxisomes found in the mother cell (Fig. 6 B). This finding is consistent with our conclusion from observations in *myo2-Y1483A* cells that Inp2p levels in the cell are regulated by peroxisome-positioning cues.

Discussion

Most intracellular movement of organelles in *S. cerevisiae* is powered by the class V myosin motor Myo2p. Interestingly, each Myo2p cargo displays Myo2p-dependent motility at a distinct time in the cell cycle. Also, the ultimate destination of Myo2p-driven transport is specific for each type of organelle (Fagarasanu et al., 2006b; Weisman, 2006). Therefore, Myo2p's attachment to and detachment from organelles are independently regulated for each type of organelle.

It is crucial to understand the structural basis for Myo2p's association with its cargoes to elucidate the regulatory mechanisms that allow it to move multiple cargoes to distinct places at different times. The regions on the surface of Myo2p required for binding two of its cargoes, namely the vacuole and secretory vesicles, have been identified (Schott et al., 1999; Catlett et al., 2000). These regions were found to be distant from one another and simultaneously exposed on the surface of the globular tail of Myo2p (Pashkova et al., 2006), suggesting that the tail does not have a major role in regulating cargo binding. Rather, the availability of cargo-specific receptors must dictate the timing of organelle attachment to Myo2p (Fagarasanu et al., 2006b; Pashkova et al., 2006; Weisman, 2006). In this study, we defined the surface region of the Myo2p tail devoted to binding peroxisomes and showed that this region is distinct from the region previously identified to bind vacuoles but partially overlaps the region that binds secretory vesicles. Recently, two surface residues that participate in vacuole binding were found to also function in the Myo2p-driven transport of mitochondria (Altmann et al., 2008). Therefore, it is likely that the yet unidentified mitochondrion-binding region of Myo2p overlaps its vacuole-binding region. These findings challenge the currently held view that the spatial segregation of various organelle-binding regions is an important feature of Myo2p, allowing it to function as a scaffold that exposes all its cargo-binding sites at the same time while still avoiding competition for the transport of different cargoes (Weisman, 2006). Overlap in the regions on the Myo2p surface specialized in binding different organelles suggests that different types of organelle could potentially compete with one another for access to Myo2p. This capacity for steric exclusion in myosin–organelle interactions would impose a tight temporal regulation on the activities of organelle-specific Myo2p receptors during the cell cycle and result in different receptors acting at different times in the inheritance of their specific organelles.

In this study, we elucidated the spatial and temporal parameters that contribute to the regulation of Inp2p, the peroxisome-specific receptor for Myo2p. The levels of Inp2p fluctuate during the cell cycle, being maximal when peroxisome inheritance occurs and decreased later in the cell cycle when about half of the peroxisomes have been delivered to the bud (Fagarasanu et al., 2006a). To gain insight into how Inp2p is regulated during the cell cycle, we followed the dynamics of Inp2p when peroxisome transfer to the bud was prevented or delayed using mutants of Myo2p that are defective in binding and transporting peroxisomes. Cells harboring such Myo2p mutants as the sole copy of Myo2p produced buds devoid of peroxisomes but still progressed normally through the cell cycle, thereby effectively dissociating

Published August 17, 2009

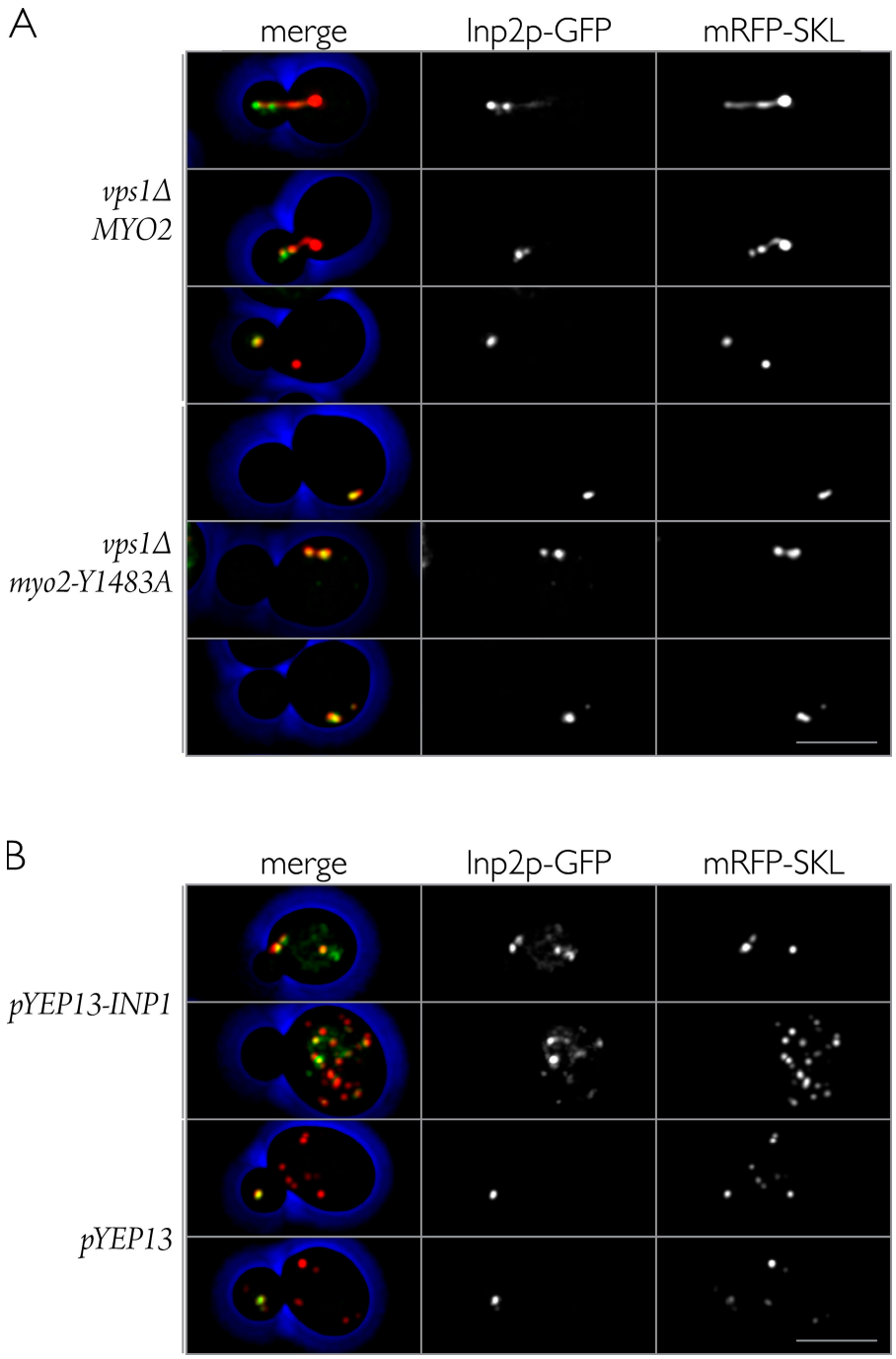

Figure 6. **Dynamics of Inp2p in cells lacking Vps1p or overproducing Inp1p.** (A) *vps1Δ* cells containing *MYO2* or the *myo2-Y1483A* allele and expressing Inp2p-GFP and peroxisomal mRFP-SKL were grown in YPD to mid-log phase, and confocal images were captured. (B) Wild-type cells expressing Inp2p-GFP and mRFP-SKL, transformed with either a multicopy YEp13 plasmid overexpressing *INP1* or YEp13 plasmid alone, were grown to mid-log phase in glucose-containing SM and examined by confocal microscopy. Left panels show the merged images of the middle and right panels. Bars, 5 µm.

the two processes of peroxisome segregation and cell cycle progression. We found that under these conditions, Inp2p levels were increased, indicating that the cellular abundance of Inp2p is not intrinsically linked to the cell cycle but rather determined by the distribution of peroxisomes in the dividing cell, i.e., by organelle positioning–specific cues. Moreover, in contrast to wild-type cells in which the Inp2p signal is highly polarized toward the bud, most peroxisomes in the mother cells of *myo2* mutants contained increased amounts of Inp2p. Therefore, the misplacement of peroxisomes caused by point mutations in the Myo2p tail influenced both the localization and levels of Inp2p. These data are consistent with a scenario in which the synthesis of Inp2p in the mother cell and its initial accumulation on a subset of peroxisomes precede its Myo2p-driven transport along with peroxisomes to the bud. In the bud, Inp2p–Myo2p transport complexes are eventually disassembled through the regulated degradation of Inp2p, releasing the transferred peroxisomes from Myo2p. Accordingly, when the association of peroxisomes with the translocation machinery is disrupted, as is the case for the *myo2* mutants with compromised peroxisome inheritance, Inp2p is protected from the bud-specific proteolytic turnover. A degradation of Inp2p in the bud to terminate peroxisome motility agrees with current models for the inheritance of other organelles, such as yeast vacuoles. Vac17p, the vacuole-specific receptor for Myo2p, was proposed to be degraded in the bud after the transfer of vacuolar membranes into the bud (Tang et al., 2003).

Published August 17, 2009

Our data are also consistent with the existence of additional regulatory mechanisms that survey the intracellular distribution of Inp2p (Fig. 7). If the increase in Inp2p levels in the *myo2* peroxisome inheritance mutants resulted exclusively from a lack of Inp2p degradation at its destination, i.e., in the bud, one would expect approximately the same number of peroxisomes to contain detectable levels of Inp2p in the wild-type and *myo2* mutant strains. However, this is not the case, as the inheritance mutant *myo2-Y1483A* displays increased amounts of Inp2p on most, if not all, peroxisomes in the mother cell. These findings strongly suggest the existence of a regulatory feedback mechanism from bud to mother cell that causes Inp2p to accumulate aberrantly on peroxisomes in the mother cell upon disruption of peroxisome inheritance (Fig. 7). Because the levels of *INP2* mRNA are essentially the same in wild-type cells and cells of the *myo2-Y1483A* mutant, this proposed feedback mechanism must operate posttranscriptionally, most likely through degradation machinery acting on Inp2p. Cellular surveillance mechanisms that monitor peroxisome partitioning could be envisioned to trigger the degradation of Inp2p in response to efficient peroxisome inheritance (Fig. 7). If the Inp2p degradation machinery is present in both mother cell and bud, its activation would not only cause the release of transferred peroxisomes from Myo2p but would also prevent new recruitments of additional peroxisomes from the mother cell. Thus, proteolytic degradation of the receptor/adaptor protein in the myosin-capturing complex could represent an effective mechanism not only for depositing a moving organelle at its proper destination (Weisman, 2006; Fagarasanu and Rachubinski, 2007; Li and Nebenführ, 2008) but also for terminating organelle inheritance.

The presence of an Inp2p signal on most peroxisomes in the mother cell was also observed when peroxisome transfer to the bud was prevented by another means, i.e., by overproduction of Inp1p. This result clearly showed that cells alter Inp2p distribution and levels in a compensatory manner in an attempt to reestablish correct peroxisome placement irrespective of the cause of the defect in peroxisome segregation. This result also demonstrated that it is not the lack of engagement of Inp2p by the Myo2p motor that leads to the changes in Inp2p distribution observed in the *myo2-Y1483A* mutant cells.

Support for this model comes from several different observations. First, the highly polarized Inp2p-GFP signal along the cell division axis in wild-type cells not only demonstrates the selectivity of Myo2p in carrying those peroxisomes that have increased amounts of Inp2p to the growing bud (Fagarasanu et al., 2006a,b) but also shows that Inp2p is not degraded as soon as it is exposed to the bud environment. The degradation of Inp2p is probably influenced by the extent of peroxisome transfer and is thus triggered after a sufficient number of peroxisomes have been partitioned to the daughter cell. Second, although the Inp2p-GFP signal in wild-type cells is not uniformly distributed among different peroxisomes, most likely all peroxisomes can acquire Inp2p, but its levels on some peroxisomes may be below the threshold of microscopic detection. Evidence to support this comes from the observation that in cells lacking the peroxisomal anchor protein Inp1p, wherein all peroxisomes have lost their ability to remain attached to the cell periphery,

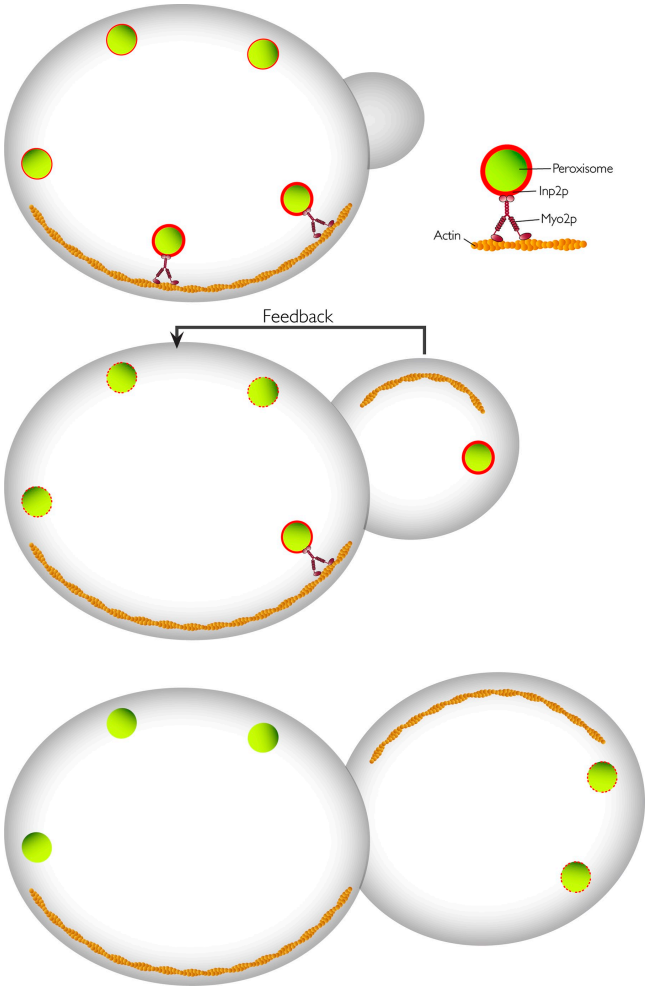

Figure 7. **A model for Inp2p regulation.** At the beginning of the cell cycle, Inp2p is loaded onto all peroxisomes. Those peroxisomes with more Inp2p have a greater probability of being carried by Myo2p into the bud. The presence of peroxisomes in the bud prevents further accumulation of Inp2p on peroxisomes remaining in the mother cell, probably by degradation of Inp2p. At the end of the cell cycle, Inp2p is turned over irrespective of peroxisome location.

the entire peroxisome population is eventually transferred to daughter cells (Fagarasanu et al., 2005), presumably in an Inp2p- and Myo2p-dependent manner (Fagarasanu and Rachubinski, 2007). This shows that in the *myo2* peroxisome inheritance mutants, the distribution of Inp2p on peroxisomes is probably similar to that found in wild-type cells, but the amount of Inp2p is increased. The delay in peroxisome partitioning in these mutants is sufficient for Inp2p levels on all peroxisomes to increase above the detection threshold, allowing for direct monitoring of how peroxisome inheritance feeds back onto Inp2p levels in the mother cell. Third, we observe a decrease in the Inp2p-GFP signal on peroxisomes in the mother cell in an inheritance mutant when peroxisomes are segregated to the bud. This suggests an inverse relationship between Inp2p levels in the mother cell and the efficiency of peroxisome transfer to the bud. Fourth, the levels of Inp2p in a peroxisome inheritance mutant, while being significantly increased, still oscillate in the cell cycle with the same pattern observed for wild-type cells. Therefore, cell cycle–related fluctuations in Inp2p levels occur irrespective of the efficiency of peroxisome inheritance. This provides further proof that

Published August 17, 2009

Inp2p turnover can occur both in the mother cell and the bud (Fig. 7). The degradation complex might be present in the cytosol or even on the peroxisomal membrane, but it appears that its activity is determined by both peroxisome positioning and cell cycle cues.

The presence of only one greatly enlarged peroxisome in cells lacking Vps1p facilitates the analysis of Inp2p dynamics because it leads to the accumulation of all Inp2p molecules in the membrane of a single peroxisome. Under these circumstances, it was evident that Inp2p-GFP initially sampled the entire peroxisome, with its leading edge containing higher levels of Inp2p. However, later in the cell cycle, only that part of the enlarged peroxisome present in the bud preserved Inp2p, and no Inp2p-GFP could be detected in the mother cell. In contrast, in cells lacking Vps1p and expressing the *myo2-Y1483A* mutation, the peroxisomes in mother cells contained detectable amounts of Inp2p. This observation is consistent with our model in which the peroxisomes that initially accumulate Inp2p, or in the case of *vps1Δ* cells, the region of the tubule that initially accumulates Inp2p, are delivered to the bud first and ultimately trigger the down-regulation of Inp2p in the peroxisomes remaining in the mother cell (Fig. 7).

Feedback regulation of Inp2p could be provided by a post-translational modification, such as phosphorylation, that would make Inp2p susceptible to degradation. In this study, we show that Inp2p is a phosphoprotein whose level of phosphorylation correlates with the cell cycle, being more pronounced at the start and end of the cell cycle. Notably, Vac17p was shown to be activated in the mother cell by phosphorylation by Cdk1p (Peng and Weisman, 2008) and in the bud by Cla4p and Ste20p, an event that leads to its turnover (Bartholomew and Hardy, 2009). The existence of two temporally distinct phosphorylation events of Inp2p hints at the possibility of successive steps of checkpoint-dependent activation and inactivation of Inp2p, such as its preparation for binding to Myo2p early in the cell cycle and its preparation for degradation late in the cell cycle. However, because the times at which the phosphorylated forms of Inp2p appear and disappear are the same in wild-type cells and cells of the peroxisome inheritance mutant *myo2-Y1483A*, the timing of phosphorylation of Inp2p is probably coupled to the cell cycle and not related to intracellular peroxisome placement.

In closing, we have shown that Inp2p, the peroxisome-specific receptor for Myo2p, is subject to both spatial and temporal regulation. Our findings point to the existence of cell cycle–dependent and organelle positioning–dependent mechanisms that control the activity and levels of organelle-specific receptors for the molecular motors that drive the intracellular motility of different membrane-bound compartments. Given that the different types of organelles compete for access to these motors, cells have developed multiple levels of regulation for their organelle-specific receptors so as to ultimately achieve an equal distribution of compartments between mother and daughter cells.

Materials and methods

Strains and culture conditions

S. cerevisiae strains used in this study are listed in Table S1. Strains were cultured at 30°C with the exception of temperature-sensitive *myo2* mutants, which were cultured at 24°C. The media components used were YPD (1% yeast extract, 2% peptone, and 2% glucose), SCIM (0.67% yeast nitrogen base without amino acids, 0.5% yeast extract, 0.5% peptone, 3.3% Brij 35, 0.3% glucose, 0.3% oleic acid, and 1× complete supplement mixture [CSM; Bio 101]), SM (0.67% yeast nitrogen base without amino acids, 2% glucose, and 1× CSM), and nonfluorescent medium (6.61 mM KH_2PO_4, 1.32 mM K_2HPO_4, 4.06 mM $MgSO_47H_20$, 26.64 mM $(NH_4)SO_4$, 1× CSM, 2% glucose, and 1% agarose).

Construction of *myo2* mutant strains

Individual point mutations in *MYO2* were made by the site-directed mutagenesis method (QuikChange; Agilent Technologies) using pRS413-MYO2 (HIS3; Pashkova et al., 2006) as a template. Each individual mutation was verified by DNA sequencing. The list of all *myo2* mutants used in this study, including ones previously made by Pashkova et al. (2006) using a similar method, is presented in Table S2.

The heterozygous deletion diploid strain *MYO2/myo2Δ* (Table S1) was transformed with pRS416-MYO2 (URA3). Successful transformants were sporulated, and tetrads were dissected to select for the haploid *MATa* strain *myo2Δ/pRS416-MYO2* (Table S1). Either the *POT1* gene encoding the peroxisomal matrix enzyme 3-ketoacyl-CoA thiolase (Pot1p) or the *INP2* gene was genomically tagged with sequence encoding an improved version of GFP (GFP+) from *Aequoria victoria* (Scholz et al., 2000) by homologous recombination with a PCR-based integrative transformation, making the strains *myo2Δ/POT1-GFP/pRS416-MYO2* and *myo2Δ/INP2-GFP/pRS416-MYO2* (Table S1). Cells of these strains were transformed with pRS413 (HIS3) containing either wild-type *MYO2* or *myo2* harboring a point mutation. Transformants were streaked onto SM lacking histidine and uracil (SM-His-Ura) to select for the presence of both plasmids and then onto SM containing 5-fluoroorotic acid to remove pRS416-MYO2. The resulting strains contained pRS413-MYO2 or pRS413-myo2 as sole copies of the *MYO2* gene. To visualize peroxisomes in strains expressing *INP2-GFP*, cells were transformed with the plasmid pmRFP-SKL encoding mRFP from *Discosoma* species (Campbell et al., 2002) tagged at its carboxyl terminus with the peroxisome-targeting signal 1, Ser-Lys-Leu. The strain *myo2Δ/vps1Δ/INP2-GFP/pmRFP-SKL/pRS413-myo2* (Table S1) was constructed by replacing the *VPS1* gene with the *LEU2* gene by homologous recombination using a PCR-based integrative transformation.

To construct the strain *myo2Δ/INP2-pA/POT1-GFP* (Table S1), *INP2* was first genomically tagged with sequence encoding *Staphylococcus aureus* pA by homologous recombination using a PCR-based integrative transformation of *myo2Δ/POT1-GFP/pRS416-MYO2* cells. A gene conferring hygromycin B resistance was substituted for the *HIS5* gene in the pA cassette using the plasmid pAG26 (Euroscarf). The pRS416-MYO2 (URA3) plasmid in the resulting strain was swapped with the pRS413 (HIS3) plasmids containing either wild-type *MYO2* or *myo2* harboring a point mutation (as described for *INP2-GFP*).

Microscopy

Cells were grown in YPD and incubated in SCIM for 16 h. Slides were prepared according to Adames et al. (2001) with modifications. Essentially, 200 µl of hot nonfluorescent medium was used to prepare a thin agarose pad on a slide with two 18-mm square wells (Cel-line Brand). 1–2 µl culture was placed onto the slide, covered with a coverslip, and sealed with Valap (1:1:1 mixture of vaseline, lanolin, and paraffin). Cells were incubated at room temperature for image capture. Images were captured as described previously (Hammond and Glick, 2000) using a modified confocal microscope equipped with a 63× 1.4 NA Plan Apo objective (LSM 510 META; Carl Zeiss, Inc.). A piezoelectric actuator was used to drive continuous objective movement, allowing for the rapid collection of *z* stacks. The sides of each pixel represented 0.057 µm of the sample. Stacks of 30–50 optical sections spaced 0.125 µm apart were captured.

Acquired images were deconvolved using algorithms provided by Huygens Professional Software (Scientific Volume Imaging BV). For this method, 3D datasets were processed to remove noise and reassign blur through an iterative classical maximum likelihood estimation algorithm and an experimentally derived point-spread function. The transmission image was treated differently. In Huygens, a Gaussian filter was applied to the transmission image, and blue color was applied to the transmission image using Imaris software (version 6.1; Bitplane, Inc.). The level of the transmission image was modified, and the image was processed until only the circumference of the cell was visible. To prevent interference of internal structures captured in the transmission images, the internal structures were removed in Photoshop (Adobe). Imaris was subsequently used to display the deconvolved 3D dataset with the processed transmission image and to prepare the image files before final figure assembly in Photoshop and InDesign (Adobe).

Published August 17, 2009

Quantification of rates of peroxisome inheritance

Rates of peroxisome inheritance were quantified essentially as described previously (Fagarasanu et al., 2005, 2006a). Cells synthesizing genomically encoded Pot1p-GFP were grown in YPD, transferred to SCIM, and incubated in SCIM for 16 h to achieve an OD_{600} of 0.5. Peroxisomes were visualized by direct fluorescence confocal microscopy. For each randomly chosen field, three optical sections of 5-µm thickness were collected at a *z* axis spacing of 1.6 µm using a high detector gain to ensure the capture of weak fluorescent signals. Optical sections were projected to a single image. All visibly budded cells were considered for analysis. Budded cells were assigned to two size categories according to bud volume expressed as a percentage of mother cell volume: category I, 0–24% (representing small-budded cells); and category II, 24–48% (representing large-budded cells). Because cell volume is not directly accessible, bud area was first measured using image browser software (LSM 5; Carl Zeiss, Inc.) and grouped into two "area" categories, which superimpose on the aforementioned "volume" categories if a spherical geometry is assumed for all cells, according to bud cross-sectional area expressed as a percentage of mother cell cross-sectional area: category I, 0–39%; and category II, 39–61%. Buds were scored using an all or none criterion for the presence or absence of peroxisomal fluorescence. Quantification was always performed on at least 50 budded cells from each category of bud size.

Staining cell structures

Yeast vacuoles were stained with *N*-(3-triethylammoniumpropyl)-(6(4(diethylamino)phenyl) hexatrienyl) pyridium dibromide (FM4-64; Invitrogen). Mitochondria were stained with the mitochondrion-selective dye chloromethyl-X-rosamine (MitoTracker red; Invitrogen) according to the manufacturer's instructions.

Assays for protein interaction

To assay direct protein interaction, GST fusion proteins of the cargo-binding domain (amino acids 1,113–1,574) of either wild-type Myo2p (GST–Myo2p) or various mutant variants of Myo2p were constructed using pGEX4T-1 (GE Healthcare). Recombinant expression and isolation of GST and GST–Myo2p were performed according to the manufacturer's instructions. MBP fusion to the soluble part of Inp2p (amino acids 241–705) was made using pMAL-c2 (New England Biolabs, Inc.) and expressed in the *E. coli* strain BL21-DE3 (EMD). 250 µg purified GST–Myo2p or GST protein immobilized on glutathione resin was incubated with 250 µg *E. coli* lysate containing an MBP fusion or MBP alone in H buffer (20 mM Hepes, pH 7.5, 60 mM NaCl, 1 mM DTT, 0.5% Triton X-100, 1 µg leupeptin/ml, 1 µg pepstatin/ml, 1 µg aprotinin/ml, 1 mM phenanthroline, and 1 mM PMSF) for 2 h at 4°C on a rocking platform. The immobilized fractions were allowed to settle and were washed three times with H buffer before protein elution in sample buffer (50 mM Tris-HCl, pH 6.8, 2% SDS, 5% glycerol, 0.001% bromophenol blue, and 5% 2-mercaptoethanol). The eluted proteins were subjected to SDS-PAGE. Immunoblotting with rabbit antibodies to MBP (New England Biolabs, Inc.) and mouse monoclonal antibodies to GST (Sigma-Aldrich) combined with Alexa Fluor 680/750–conjugated goat anti–mouse/anti–rabbit antibodies (Invitrogen) was used to detect protein interactions in the assay for direct protein binding. Immunoblots were processed using a digital imaging system (Odyssey; LI-COR Biosciences) with the resolution set to 84 µm and the highest quality and involved an initial subtraction of the background signal from the GST-only lane and subsequent normalization to the signal of the background-corrected wild-type Myo2p. Yeast two-hybrid analysis was performed as described previously (Ishikawa et al., 2003).

Cell cycle arrest

α Factor–induced G1 arrest was performed as described previously (Fagarasanu et al., 2005, 2006a). Cells grown in YPD to early log phase were synchronized by treatment with 1 µg α factor (Sigma-Aldrich)/ml for 2 h. Cell cycle arrest was monitored by microscopic examination of cells. Arrested cells were washed with fresh medium twice to remove α factor and incubated in fresh medium at 23°C. Equal amounts of cells were collected at each time point as indicated, and total cell lysates were subjected to SDS-PAGE.

Alkaline phosphatase treatment

To obtain whole cell lysates for alkaline phosphatase treatment, 10 OD_{600} U cells in early log phase (OD_{600} = ~0.3) were harvested, washed once with water, and resuspended in 1 ml of water. Total protein was precipitated by successive addition of 150 µl 2 N NaOH, 5% 2-mercaptoethanol, and 100 µl 50% TCA followed by incubation on ice for 30 min. Alkaline phosphatase treatment was performed essentially as described previously (Peng and Weisman, 2008). In brief, protein pellets were resuspended in 140 µl 0.3 M sorbitol, 10 mM Tris-HCl, pH 7.5, 0.1 M NaCl, 1 mM $MgCl_2$, and 1 mM EDTA, and 60 µl 1 M Tris base, 133 µl 10% SDS, and 7 µl 2-mercaptoethanol were added. 100 µl of these lysates were diluted with 900 µl 50 mM Tris-HCl, pH 8.8. Phosphatase reactions were started by addition of 20 U calf intestine alkaline phosphatase (0.5 U/µl; New England Biolabs, Inc.) and incubated at 30°C for 1 h. Total protein was precipitated for 30 min on ice by addition of 50% TCA to a final concentration of 15% and pelleted by centrifugation. Protein pellets were dissolved in 20 µl 1 M Tris base and 100 µl 2× SDS sample buffer (150 mM Tris-HCl, pH 6.8, 15% glycerol, 2% SDS, 4% 2-mercaptoethanol, and bromophenol blue [trace]) and boiled before SDS-PAGE.

Antibodies

Inp2p-pA was detected by immunoblotting with affinity-purified rabbit IgG (MP Biomedicals). Rabbit antibodies to *S. cerevisiae* glucose-6-phosphate dehydrogenase (G6PDH) were obtained from Sigma-Aldrich. Rabbit antibodies to Clb2p were provided by R. Wozniak (University of Alberta, Edmonton, Alberta, Canada). Horseradish peroxidase–conjugated donkey anti–rabbit IgG secondary antibodies were used to detect primary antibodies in immunoblot analysis. Antigen–antibody complexes in immunoblots were detected by enhanced chemiluminescence (GE Healthcare).

Northern analysis

Total RNA was extracted with hot acidic phenol. Contaminating chromosomal DNA was removed by treatment with DNase I, and 30 µg RNA was separated in 1.25% agarose gels containing 6% formaldehyde. RNA was blotted onto nylon membranes (GE Healthcare) in 20× SSC and cross-linked to the membrane by transillumination. Blots were hybridized under stringent conditions in Rapid-hyb buffer (GE Healthcare) with *INP2*- and *ACT1*-specific probes, which were ^{32}P radiolabeled using the Prime-It II random primer labeling kit (Agilent Technologies). Blots were washed in 50% formamide and subjected to autoradiography.

Additional method

All figures showing the Myo2p protein structure were made using PyMOL software (http://www.pymol.org).

Online supplemental material

Table S1 lists the *S. cerevisiae* strains used in this study. Table S2 lists the *myo2* point mutants used in this study. Online supplemental material is available at http://www.jcb.org/cgi/content/full/jcb.200904050/DC1.

We thank Richard Poirier, Dwayne Weber, Hanna Kroliczak, and Elena Savidov for technical help. We also thank Drs. Neil Adames and Howard Young and the members of the Rachubinski laboratory for helpful discussions.

A. Fagarasanu was supported by a Studentship from the Alberta Heritage Foundation for Medical Research (AHFMR). F.D. Mast was supported by a Canada Graduate Scholarship from the Canadian Institutes of Health Research (CIHR) and a Faculty of Medicine and Dentistry 75th Anniversary Award. G.A. Eitzen holds a New Investigator award from the CIHR and is an AHFMR Scholar. R.A. Rachubinski is an International Research Scholar of the Howard Hughes Medical Institute. This work was supported by grant 9208 from the CIHR to R.A. Rachubinski and by grants R01-GM75152 and R01-GM62261 from the National Institutes of Health to J.D. Aitchison and L.S. Weisman, respectively.

Submitted: 9 April 2009
Accepted: 15 July 2009

References

Adames, N.R., J.R. Oberle, and J.A. Cooper. 2001. The surveillance mechanism of the spindle position checkpoint in yeast. *J. Cell Biol.* 153:159–168.

Altmann, K., M. Frank, D. Neumann, S. Jakobs, and B. Westermann. 2008. The class V myosin motor protein, Myo2, plays a major role in mitochondrial motility in *Saccharomyces cerevisiae*. *J. Cell Biol.* 181:119–130.

Arai, S., Y. Noda, S. Kainuma, I. Wada, and K. Yoda. 2008. Ypt11 functions in bud-directed transport of the Golgi by linking Myo2 to the coatomer subunit Ret2. *Curr. Biol.* 18:987–991.

Bartholomew, C.R., and C.F. Hardy. 2009. The p21-activated kinases Cla4 and Ste20 regulate vacuole inheritance in *S. cerevisiae*. *Euk. Cell.* In press.

Beach, D.L., J. Thibodeaux, P. Maddox, E. Yeh, and K. Bloom. 2000. The role of the proteins Kar9 and Myo2 in orienting the mitotic spindle of budding yeast. *Curr. Biol.* 10:1497–1506.

Boldogh, I.R., S.L. Ramcharan, H.C. Yang, and L.A. Pon. 2004. A type V myosin (Myo2p) and a Rab-like G-protein (Ypt11p) are required for retention of newly inherited mitochondria in yeast cells during cell division. *Mol. Biol. Cell.* 15:3994–4002.

Bretscher, A. 2003. Polarized growth and organelle segregation in yeast: the tracks, motors, and receptors. *J. Cell Biol.* 160:811–816.

Campbell, R.E., O. Tour, A.E. Palmer, P.A. Steinbach, G.S. Baird, D.A. Zacharias, and R.Y. Tsien. 2002. A monomeric red fluorescent protein. *Proc. Natl. Acad. Sci. USA.* 99:7877–7882.

Catlett, N.L., and L.S. Weisman. 1998. The terminal tail region of a yeast myosin-V mediates its attachment to vacuole membranes and sites of polarized growth. *Proc. Natl. Acad. Sci. USA.* 95:14799–14804.

Catlett, N.L., J.E. Duex, F. Tang, and L.S. Weisman. 2000. Two distinct regions in a yeast myosin-V tail domain are required for the movement of different cargoes. *J. Cell Biol.* 150:513–526.

Estrada, P., J. Kim, J. Coleman, L. Walker, B. Dunn, P. Takizawa, P. Novick, and S. Ferro-Novick. 2003. Myo4p and She3p are required for cortical ER inheritance in *Saccharomyces cerevisiae. J. Cell Biol.* 163:1255–1266.

Fagarasanu, A., and R.A. Rachubinski. 2007. Orchestrating organelle inheritance in *Saccharomyces cerevisiae. Curr. Opin. Microbiol.* 10:528–538.

Fagarasanu, M., A. Fagarasanu, Y.Y.C. Tam, J.D. Aitchison, and R.A. Rachubinski. 2005. Inp1p is a peroxisomal membrane protein required for peroxisome inheritance in *Saccharomyces cerevisiae. J. Cell Biol.* 169:765–775.

Fagarasanu, A., M. Fagarasanu, G.A. Eitzen, J.D. Aitchison, and R.A. Rachubinski. 2006a. The peroxisomal membrane protein Inp2p is the peroxisome-specific receptor for the myosin V motor Myo2p of *Saccharomyces cerevisiae. Dev. Cell.* 10:587–600.

Fagarasanu, M., A. Fagarasanu, and R.A. Rachubinski. 2006b. Sharing the wealth: peroxisome inheritance in budding yeast. *Biochim. Biophys. Acta.* 1763:1669–1677.

Fagarasanu, A., M. Fagarasanu, and R.A. Rachubinski. 2007. Maintaining peroxisome populations: a story of division and inheritance. *Annu. Rev. Cell Dev. Biol.* 23:321–344.

Govindan, B., R. Bowser, and P. Novick. 1995. The role of Myo2, a yeast class V myosin, in vesicular transport. *J. Cell Biol.* 128:1055–1068.

Hammond, A.T., and B.S. Glick. 2000. Raising the speed limits for 4D fluorescence microscopy. *Traffic.* 1:935–940.

Hoepfner, D., M. van den Berg, P. Philippsen, H.F. Tabak, and E.H. Hettema. 2001. A role for Vps1p, actin, and the Myo2p motor in peroxisome abundance and inheritance in *Saccharomyces cerevisiae. J. Cell Biol.* 155:979–990.

Ishikawa, K., N.L. Catlett, J.L. Novak, F. Tang, J.J. Nau, and L.S. Weisman. 2003. Identification of an organelle-specific myosin V receptor. *J. Cell Biol.* 160:887–897.

Itoh, T., A. Watabe, A. Toh-E, and Y. Matsui. 2002. Complex formation with Ypt11p, a rab-type small GTPase, is essential to facilitate the function of Myo2p, a class V myosin, in mitochondrial distribution in *Saccharomyces cerevisiae. Mol. Cell. Biol.* 22:7744–7757.

Itoh, T., A. Toh-E, and Y. Matsui. 2004. Mmr1p is a mitochondrial factor for Myo2p-dependent inheritance of mitochondria in the budding yeast. *EMBO J.* 23:2520–2530.

Li, J.F., and A. Nebenführ. 2008. The tail that wags the dog: the globular tail domain defines the function of myosin V/XI. *Traffic.* 9:290–298.

Lipatova, Z., A.A. Tokarev, Y. Jin, J. Mulholland, L.S. Weisman, and N. Segev. 2008. Direct interaction between a myosin V motor and the Rab GTPases Ypt31/32 is required for polarized secretion. *Mol. Biol. Cell.* 19:4177–4187.

Pashkova, N., N.L. Catlett, J.L. Novak, G. Wu, R. Lu, R.E. Cohen, and L.S. Weisman. 2005. Myosin V attachment to cargo requires the tight association of two functional subdomains. *J. Cell Biol.* 168:359–364.

Pashkova, N., Y. Jin, S. Ramaswamy, and L.S. Weisman. 2006. Structural basis for myosin V discrimination between distinct cargoes. *EMBO J.* 25:693–700.

Peng, Y., and L.S. Weisman. 2008. The cyclin-dependent kinase Cdk1 directly regulates vacuole inheritance. *Dev. Cell.* 15:478–485.

Pruyne, D., A. Legesse-Miller, L. Gao, Y. Dong, and A. Bretscher. 2004. Mechanisms of polarized growth and organelle segregation in yeast. *Annu. Rev. Cell Dev. Biol.* 20:559–591.

Reck-Peterson, S.L., D.W. Provance Jr., M.S. Mooseker, and J.A. Mercer. 2000. Class V myosins. *Biochim. Biophys. Acta.* 1496:36–51.

Rossanese, O.W., C.A. Reinke, B.J. Bevis, A.T. Hammond, I.B. Sears, J. O'Connor, and B.S. Glick. 2001. A role for actin, Cdc1p, and Myo2p in the inheritance of late Golgi elements in *Saccharomyces cerevisiae. J. Cell Biol.* 153:47–62.

Scholz, O., A. Thiel, W. Hillen, and M. Niederweis. 2000. Quantitative analysis of gene expression with an improved green fluorescent protein. p6. *Eur. J. Biochem.* 267:1565–1570.

Schott, D., J. Ho, D. Pruyne, and A. Bretscher. 1999. The COOH-terminal domain of Myo2p, a yeast myosin V, has a direct role in secretory vesicle targeting. *J. Cell Biol.* 147:791–808.

Tang, F., E.J. Kauffman, J.L. Novak, J.J. Nau, N.L. Catlett, and L.S. Weisman. 2003. Regulated degradation of a class V myosin receptor directs movement of the yeast vacuole. *Nature.* 422:87–92.

Weisman, L.S. 2003. Yeast vacuole inheritance and dynamics. *Annu. Rev. Genet.* 37:435–460.

Weisman, L.S. 2006. Organelles on the move: insights from yeast vacuole inheritance. *Nat. Rev. Mol. Cell Biol.* 7:243–252.

Yin, H., D. Pruyne, T.C. Huffaker, and A. Bretscher. 2000. Myosin V orientates the mitotic spindle in yeast. *Nature.* 406:1013–1015.